REPORT DOCUMENTATION PAGE			Form Approved OMB No. 0704-0188

1. AGENCY USE ONLY *(Leave blank)*	2. REPORT DATE	3. REPORT TYPE AND DATES COVERED
	8.Aug.00	THESIS

4. TITLE AND SUBTITLE
FORECASTING THE ONSET OF CLOUD-GROUND LIGHTNING USING LAYERED VERTICALLY INTEGRATED LIQUID WATER

5. FUNDING NUMBERS

6. AUTHOR(S)
CAPT DARCANGELO DAVID L

7. PERFORMING ORGANIZATION NAME(S) AND ADDRESS(ES)
PENNSYLVANIA STATE UNIVERSITY

8. PERFORMING ORGANIZATION REPORT NUMBER

9. SPONSORING/MONITORING AGENCY NAME(S) AND ADDRESS(ES)
THE DEPARTMENT OF THE AIR FORCE
AFIT/CIA, BLDG 125
2950 P STREET
WPAFB OH 45433

10. SPONSORING/MONITORING AGENCY REPORT NUMBER
FY00-263

11. SUPPLEMENTARY NOTES

12a. DISTRIBUTION AVAILABILITY STATEMENT
Unlimited distribution
In Accordance With AFI 35-205/AFIT Sup 1

12b. DISTRIBUTION CODE

13. ABSTRACT *(Maximum 200 words)*

14. SUBJECT TERMS

15. NUMBER OF PAGES
60

16. PRICE CODE

17. SECURITY CLASSIFICATION OF REPORT	18. SECURITY CLASSIFICATION OF THIS PAGE	19. SECURITY CLASSIFICATION OF ABSTRACT	20. LIMITATION OF ABSTRACT

The Pennsylvania State University

The Graduate School

Department of Meteorology

FORECASTING THE ONSET OF CLOUD-GROUND LIGHTNING USING LAYERED VERTICALLY INTEGRATED LIQUID WATER

A Thesis in

Meteorology

by

David L. D'Arcangelo

Submitted in Partial Fulfillment
of the Requirements
for the Degree of

Master of Science

August 2000

I grant The Pennsylvania State University the nonexclusive right to use this work for the University's own purposes and to make single copies of the work available to the public on a not-for-profit basis if copies are not otherwise available.

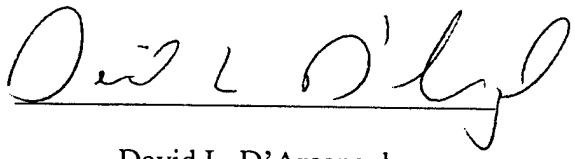

David L. D'Arcangelo

We approve the thesis of David L. D'Arcangelo

Date of Signature

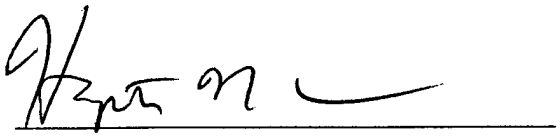

13 July 2000

Hampton N. Shirer
Associate Professor of Meteorology
Thesis Advisor

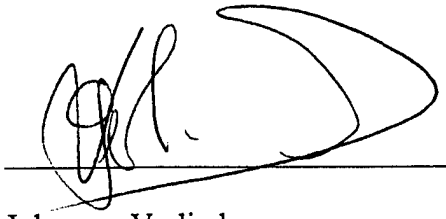

7/12/2000

Johannes Verlinde
Associate Professor of Meteorology

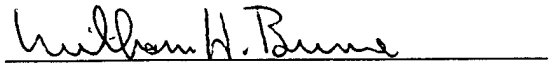

12 July 2000

William H. Brune
Professor of Meteorology
Head of the Department of Meteorology

ABSTRACT

Accurate forecasting of cloud-ground (CG) lightning onset at the Kennedy Space Center (KSC), Florida is critical for personnel safety, but presents a difficult problem. Current methods for predicting CG lightning onset rely on radar analyses that require a reflectivity threshold to be exceeded at a specified temperature level. Although the requisite temperature level used in lightning forecasting lies within the critical region of convection for lightning initiation (-10 to -20°C), current methods of prediction do not employ a complete description of the storm structure. This thesis hypothesizes that diagnosing the storm structure within the -10 to -20°C layer is a key element in forecasting lightning onset. This storm structure can readily be described by the variation of the liquid water content, termed layered vertically integrated liquid (LVIL), within two layers in the supercooled region (-10 to -15°C and -15 to -20°C). An LVIL value for each layer, described together as a threshold pair, quantifies the minimum vertical structure required for lightning onset. The optimal threshold pair follows from weighting measures of forecast skill; in order of importance, they are probability of detection (POD), Kuipers skill score (KSS) and false alarm rate (FAR). LVIL amounts of 0.5 mm in the -10 to -15°C layer coinciding with amounts of 0.25 mm in the -15 to -20°C layer indicate that lightning is imminent, with a POD of 96%, a KSS of 51% and a FAR of 21%. This two-layer approach is superior to one-parameter methods currently in use at the KSC.

TABLE OF CONTENTS

LIST OF FIGURES

LIST OF TABLES

ACKNOWLEDGMENTS

I would like to take this opportunity to thank my advisor, Dr. Hampton N. Shirer, for his support, advice and patience throughout this project. He has always pushed the right amount in the direction I needed most. In addition, he has listened to my many trials and tribulations, many of which did not involve academic pursuits. I will always be grateful for his encouragement and for being a major part of the success of this project.

I also want to thank Dr. Hans Verlinde, my second advisor. His discussions on radar topics and about "pulse" convection were invaluable. Bill Roeder, Chief Staff Meteorologist at KSC, deserves special credit for shaping this work and offering many suggestions and ideas along the way. He convinced me that LVIL was worth pursuing and constructed the framework for what was to be a very rewarding experience. My only regret is that I did not have the opportunity to work with him at the 45th Weather Squadron. Pete Speck and Danny Kerupetski at the Air Force Combat Climatology Center deserve thanks for supplying the NLDN and sounding data. Dr. Greg Forbes collected and endowed the radar data to me. Rich Grumm, Science and Operations Officer at the State College National Weather Service Office, was helpful in manipulating and interpreting the WATADS data.

The Air Force Institute of Technology deserves thanks for initiating and supporting my graduate endeavors. I have received more from the Air Force than I could return in a lifetime of service.

A special place in my heart is reserved for my wife Stephanie and my two sons, Ethan and Benjamin, for their unwavering support and unconditional love. Stephanie always keeps me believing and focused while the boys are a constant source of joy. I love the fact that no matter what kind of day I've had they always want to play games with dad when I get home. Their youthful exuberance keeps everything in perspective. I also want to thank my parents and my in-laws for always believing this work would someday be a finished product and I would be a better person for it.

Chapter 1

INTRODUCTION

Accurate prediction of lightning, both spatially and temporally, is crucial to the mission of the 45th Weather Squadron (WS) at Patrick Air Force Base (PAFB), FL. The 45th WS is responsible for operational weather services along the east-central coast of Florida, at both Cape Canaveral Air Force Station (CCAFS) and the National Aeronautics and Space Administration (NASA) Kennedy Space Center (KSC). Weather watches and warnings at these two locations are issued to protect over 25,000 personnel and facility resources worth $7 billion, which does not include the vehicles and their payloads at the KSC complex (Boyd et al. 1995).

Lightning has a dramatic impact on activities around the KSC complex. For example, the area of maximum thunderstorm occurrence in the United States is in Central Florida, not far from the KSC complex (Hodanish et al. 1997). In addition, numerous weather-sensitive outdoor activities are required prior to space launch, such as transporting vehicles/payloads; moving, stacking, and destacking solid rocket motors; and fueling/defueling vehicles (Boyd et al. 1995). Circumstances such as these require fine-scale, highly accurate prediction of the onset of cloud-ground (CG) lightning around the KSC. A study by Roeder et al. (2000) finds that weather delayed or scrubbed 27.5% of launch attempts at KSC, over 466 countdowns from 1 Oct 1988 – 30 Sep 1999. In addition, lightning delayed or scrubbed 8.2% of all countdowns, making it second to upper level winds (8.6% of all countdowns) in causes of weather impacts (Roeder et al.

2000). Furthermore, the delays in launch preparation and costs incurred from lightning watches and warnings and for personnel safety and resource protection, although not documented, are significant. In fact, the prime motivation for this research is personnel safety and resource protection, while the decrease in launch delays is only a secondary motivation. Some launch delays are for triggered lightning threats not CG lightning. However, CG lightning provides the sole threat to personnel and ground equipment.

Cloud-ground lightning around KSC for the summer months of June to September, which accounts for 90% of the annual total, varies from around 10 strikes per square kilometer on the coast to more than 30 in an area just beginning about 8 miles west of the Shuttle Landing Facility (Hodanish et al. 1997). Figure 1.1 shows this maximum area as it extends west across the Florida peninsula. Ten years of hourly, summer climatology for the Shuttle Landing Facility (Boyd et al. 1995) reveals that the thunderstorm maximum occurs during the afternoon, reaching a peak of 17% of the hourly observations from 3 pm to 5 pm Local Standard Time in August. The second-most frequent observation is from noon to 2 pm Local Standard Time, with 13% of the observations reporting a thunderstorm.

The high frequency of thunderstorms over and to the west of KSC is a result of the subtle, complex weather in Central Florida. The local land/water distribution and the resultant temperature differences between the Atlantic Ocean and numerous bays, inlets and lakes, create a complicated frictional/stability environment (Roeder et al. 2000). When the prevailing flow is easterly, as it often is during the summer, the major driver of

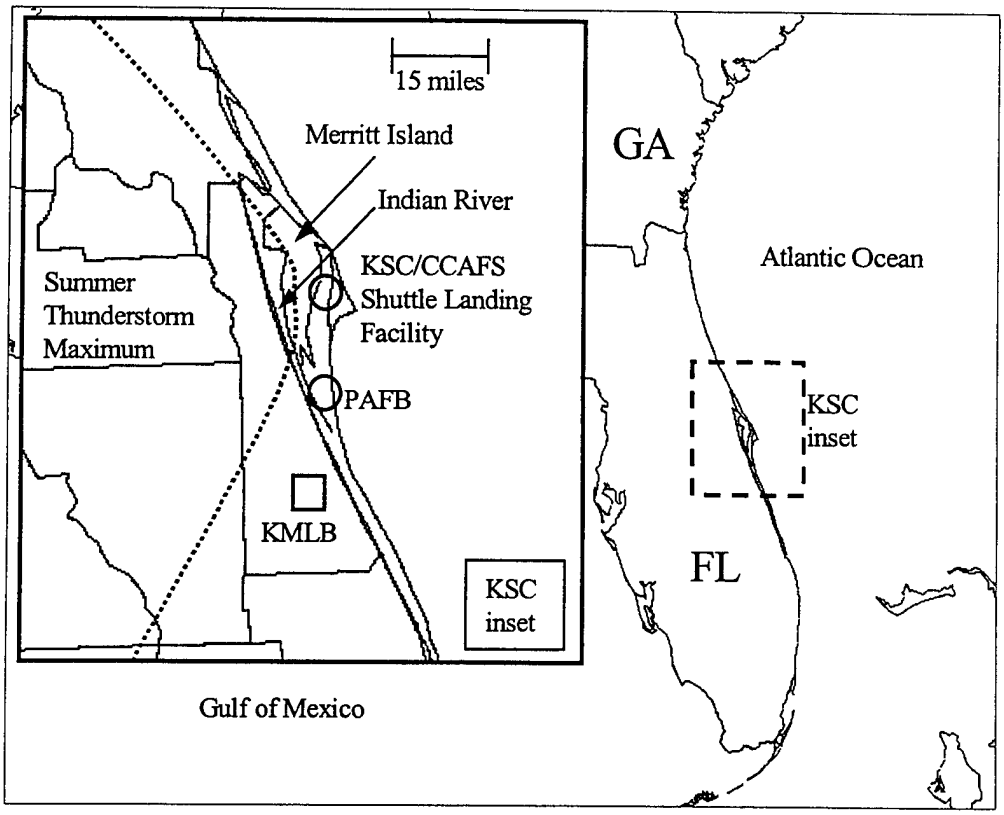

Figure 1.1. Map of Southeast United States coast with inset of the KSC region. Note the summer thunderstorm maximum located just west of the KSC and shuttle landing facility.

summer thunderstorm formation is the East Coast Sea-Breeze (ECSB), forming along the coast by mid to late morning and moving inland during the afternoon. The local thunderstorm maximum just west of KSC (see fig. 1.1) is the result of local convergence of two sea breezes caused by the irregular shape of Cape Canaveral protruding into the Atlantic Ocean (Hodanish 1997). Occasionally, when the prevailing flow is westerly, the West Coast Sea-Breeze (WCSB), induced by the temperature difference between the Gulf of Mexico and the Florida peninsula, collides with the ECSB and triggers numerous thunderstorms over the Florida peninsula. The intricacies of the ECSB and the WCSB and their importance in localized thunderstorm development are well documented by Neumann (1968, 1971). Rao (1999) also finds that the vertical motions from the Indian River Sea Breeze, a much smaller body of water west of KSC, are as strong as the ECSB itself. In addition, there are many other mesoscale features that can contribute to thunderstorm formation: convective outflows, horizontal convective rolls, cloud shadow and soil moisture temperature discontinuities and remnants of boundaries from previous day(s) etc. (Lopez and Holle 1987; Roeder et al. 2000). Thus, the weak features leading to thunderstorm formation, secondary factors in other locations, can dominate the summer patterns of Central Florida.

1.1 Lightning Warnings at the KSC

The 45th WS provides two levels of lightning advisories for 5 nm circles for 13 operationally significant sites at KSC, PAFB and CCAFS (Roeder et al. 1998). The first

level, a lightning "watch," is issued when lightning is expected within 30 minutes. Summertime thunderstorms develop too rapidly to rely heavily on radar analysis for issuance of a watch. In fact, one half of the lightning-producing storms studied in this thesis existed for 10 minutes or less between the time of first detection and the first CG flash. Thus, issuing a watch relies more on high-resolution satellite analyses and surface convergence trends diagnosed from the local weather tower network. The second advisory level, a lightning "warning," is issued for imminent or occurring lightning. The issuance of a lightning warning relies most heavily on radar analysis.

KSC uses two radar systems to evaluate lightning threat. The primary radar for lightning forecasting is a WSR-74C located at KSC and operated by the United States Air Force. The WSR-74C employs a 2.5-minute scan strategy and 12 elevation angles from 0.5° to 25.9° (Boyd et al. 1999). The backup radar system is a National Weather Service WSR-88D, located 25 nm SSW of KSC, at the Melbourne (KMLB in figure 1.1) National Weather Service forecast office. The WSR-88D uses a 5- to 6-minute scan strategy with 9 to 14 elevation angles, depending upon volume coverage pattern, from 0.5° to 19.5°.

There are two radar techniques used at KSC to evaluate the onset of CG lightning. The first empirical rule uses a threshold of 45 dBZ at the -10°C level (Roeder et al. 1998). This rule mandates that the 45 dBZ echo must extend above the -10°C level for at least 3000' and exist for 10- to 15-minutes. This rule, a 45th WS local rule-of-thumb for lightning forecasting, is called the 'Pinder Principle' (Roeder and Pinder 1998), named after Mr. Clark Pinder, the local lightning/radar expert, provides operational forecasters

guidance for nowcasting lightning. The second, experimental technique takes advantage of the WSR-74C Integrated Radar Information System (IRIS) post-processor and display system from Sigmet Inc., which can use reflectivity data to derive layered vertically integrated liquid (LVIL) amounts in the 0 to -20°C layer or other user specified layers. These LVIL amounts are given in millimeters (mm). The more commonly used vertically integrated liquid (VIL) algorithm of the WSR-88D uses units of kilograms per square meter, which is related to LVIL through the density of water, however, their magnitudes are the same. For consistency with the LVIL product at the KSC, this study uses the units of mm. Based on theory and local experience, the 45th WS initially created an experimental WSR-74C/IRIS lightning forecast product based on LVIL above the summer climatological freezing level height for the CCAFS sounding. Preliminary studies during the 1999 summer thunderstorm season indicate an LVIL of 4 mm (equivalent to 4 kg m^{-2} using the WSR-88D algorithm) between the 0 and -20°C levels is an indicator of imminent CG lightning (Pinder, 45th WS internal memo, 1998). However, no statistics were generated on 1999 storms using this approach. This study tests the Pinder Principle and the 4 mm rule employed by the 45th WS as baselines leading to the development of a finer resolution LVIL CG forecast algorithm. In addition, the 0 to -20°C layer is divided into 5°C layers, with the utility of LVIL evaluated for all layers and combinations thereof.

1.2 Lightning Onset

Observational studies of the cloud electrification process show the center of negative charge, which is necessary to initiate a lightning discharge, is typically located in the supercooled region of the cloud. Until the mid 1990s, observational studies of lightning initiation relied on analysis of radar reflectivity data and electric field measurements from aircraft. Present empirical forecasting techniques for the onset of CG lightning are largely based on these early studies. Table 1.1 provides a summary of the studies cited in this section and includes an assessment of the result of this thesis.

A 1984 New Mexico field study finds that the initial point charges in thunderstorms are located between -3 to -15°C with a reflectivity core of > 30 dBZ in all storms (Breed et al. 1989). Further examination of the New Mexico results shows that the electrical enhancement and subsequent lightning discharge occurs only when reflectivities exceed 40 dBZ at about the -10°C level (Dye et al. 1989). Similarly, but in a different region, Buechler and Goodman's (1990) study of Midwest storms finds that lightning is imminent when the 40 dBZ echo reached the -10°C level. Analogously, Michimoto (1991, 1993), in a study of thunderstorms in Japan, shows that the first lightning discharge occurs 5 to 30 minutes after the 30 dBZ echo reached -20°C. From the New Mexico results and earlier studies of electrified cumulonimbus in Montana, Dye (1986, 1989) hypothesizes that collisions between graupel and ice particles are necessary to initiate electrification. Moreover, Dye (1986) and Ziegler (1986) suggests that the

Summary of Lightning Initiation Signatures				
Study	Years/Locations	Threshold (dBZ unless noted)	Temp (°C) Threshold	Assessment
Breed and Dye	1984/NM	30	-3 to -15	6 storms, not focused on reflectivity at one level
Dye et al.	1984/NM	40	-10	20 storms, detailed analysis of continental clouds
Buechler et al.	1990/FL, AL, NM	40	-10	15 storms, POD 100%, FAR 7%, 4-33 minute leadtime
Michimoto	1991/Japan	30	-20	analysis included winter convection
Hondl and Eilts	1990/FL	10	0	POD 100%, FAR 41%
Gremillion	1989-96/FL	30	-15	results not reproducible on VIL database
Pinder	ongoing/FL	45	-10	current KSC tecnique
KSC	ongoing/FL	4mm (LVIL)	0 to -20	KSC experimental technique
Jameson et al.	1991/FL	2mm (drop size)	-7	used dual frequency, dual polarization radar
This thesis	1993-97/FL	0.50mm/0.25mm (LVIL)	-10 to -15/-15 to -20	POD 96%, FAR 21%, KSS 51%

Table 1.1. A summary of lightning initiation signatures from previous studies. Probability of Detection (POD), False Alarm Rate (FAR), and Kuipers Skill Score (KSS) are defined by equations 3, 4 and 5 in chapter 2.

updraft-downdraft transition zone between -10 and -20°C might be a preferred location or charge generation.

Hondl and Eilts (1994) used Doppler radar to examine thunderstorms in Central Florida to find that the 10 dBZ echo, when first detected near the freezing level, is a lightning initiation signature. Observed leadtimes between this signature and the first detected CG discharge range from 5 to 45 minutes, with a median leadtime of 15 minutes (Hondl and Eilts 1994). Although all 22 lightning-producing storms in the Hondl and Eilts study met the 10 dBZ at 0°C threshold, 15 other storms that met the threshold did not produce lightning. This result suggests that a better probability of detection might be obtained by examining radar signatures extending higher into the supercooled layer, as found in other regions in the above studies by Buechler, Dye and Ziegler. In an attempt to refine the 'Pinder Principle', Gremillion (1998) studied Florida storms and finds the 30 dBZ echo detected near the -15°C temperature height to be the best indicator of the beginning of CG lightning activity. The Pinder Principle and Gremillion's result are tested against the database used in this thesis. Both empirical rules are outperformed by the LVIL threshold criteria developed in this thesis. In addition, Gremillion's results are not reproducible using the LVIL database. These results are explained in detail in chapter 3.

A study of pulse (i.e. airmass) convection in Florida using the NCAR dual-frequency, dual-polarization CP-2 radar shows that the onset of electrification occurs simultaneously with raindrops larger than 2 mm above the -7°C level (Jameson et al.

1996). These drops are accompanied by significant depolarization, indicating the freezing of these drops and subsequent production of the first graupel. This freezing likely leads to rapid production of smaller ice particles and the initiation of electrification.

Heckman (1999) presents recent results from the Tropical Rainfall Measuring Mission (TRMM) satellite that suggest the source of large electric potential gradient (expressed by Heckman as power density) in thunderstorms is concentrated 1 to 2 kilometers above the freezing level. TRMM maps a single snapshot of radar reflectivity and 80 seconds of lightning locations. Heckman (1999) maps the power density to relate radar reflectivity profiles to lightning flash rates. Although the results are still preliminary, Heckman suggests his results show that lightning rate is proportional to the volume of the storm located above 25 dBZ and above the freezing level.

The strength of a convective storm and the amount of CG lightning activity are related to the vertical profile of reflectivity (VPR) in two previous studies (Robinson et al. 1997; Zipser et al. 1994). Those two projects relate the vertical velocity in the supercooled layer to the change in reflectivity with height; however, they do not examine the correlation between VPR and the onset of CG lightning. Both studies find strong vertical velocities associated with strong convective lines are linked to high CG flash rates; thus, there appears to be a distinct advantage in using the vertical structure of reflectivity to predict the onset of CG lightning.

Thus, Heckman's results, like those for earlier studies, suggest incorporating the depth of reflectivity to help predict the onset of lightning. The variability in the results of

table 1.1 suggests another factor is needed to resolve the apparent discrepancies of employing one reflectivity at one threshold to predict lightning initiation. Therefore, this thesis takes an integrated approach to the problem by examining the utility of the vertical structure of LVIL in the supercooled layer as a predictor of CG lightning onset.

Chapter 2

METHODOLOGY

In this thesis, layered vertically integrated liquid (LVIL) water is calculated in the supercooled layer from 0 to -20°C. Included in this study are 79 pulse storms across east-central Florida for the summer months 1993 to 1997. This chapter focuses on the technique used to calculate LVIL and how it is applied for developing a reliable algorithm to forecast the onset of CG lightning.

2.1 Radar Data

The primary radar used at the KSC to evaluate lightning potential is the WSR-74C. Unfortunately, there is no archive of WSR-74C data; therefore, this thesis relies upon level II archive data from the National Weather Service WSR-88D from Melbourne, FL (KMLB). This 10 cm wavelength radar uses a 5- to 6-minute scan strategy with fixed elevation angles ranging from 0.5 to 19.5° (Crum et al. 1993). The level II archive data used in this study were processed, analyzed and displayed by the WSR-88D Algorithm Testing and Display System (WATADS) developed at the National Severe Storms Laboratory (McKibben 1995).

Only pulse storms are analyzed in this study. A pulse storm is defined as an isolated cell with one distinct reflectivity core. Pulse convection is designated using WATADS through the Storm Cell Identification and Tracking (SCIT) algorithm (Johnson et al. 1998). SCIT is intended to track individual reflectivity cores and project their

movement through an initial storm motion vector. For simplicity in tracking developing, pulse convection, the SCIT algorithm is allowed to define pulse storms through a single storm identification number. Figure 2.1 is an example from 25 Jun 1993 of several storm cells west of KSC. The beam elevation angle is 0.5° and the panel is centered 10 nm west of KSC. The SCIT algorithm has identified three cells and numbered them 37, 56 and 62. Cell 56 would be a candidate for this study because it is isolated and is identified by only one number. If cell 56 were to split into two cells with two new identification numbers before the first CG flash occurs then it would not be included in this study. The area of convection identified by cells 37 and 62 does not constitute a pulse storm because of the clustered nature and proximity of two SCIT IDs within the same parent cell. Consequently, the cluster denoted by cells 37 and 62 would not be included in this study. Similarly, lines of convection and merging or splitting cells with numerous SCIT IDs are not considered pulse storms and so are not included in the development of the LVIL CG forecasting algorithm. Only isolated cells with a single SCIT ID up to and including the time of first CG flash are considered for this study.

Unfortunately, the evolution of convective development in summertime Florida is only marked by true pulse convection during the early part of the day (late morning to early afternoon). After convection has been underway for several hours, there is a tendency for clustering of the convection, with new cells forming alongside areas or lines of older cells. Thus, the vast majority of cells considered in this study occurred early in a convective day. Once the scene has been filled with clusters of convection, CG lightning

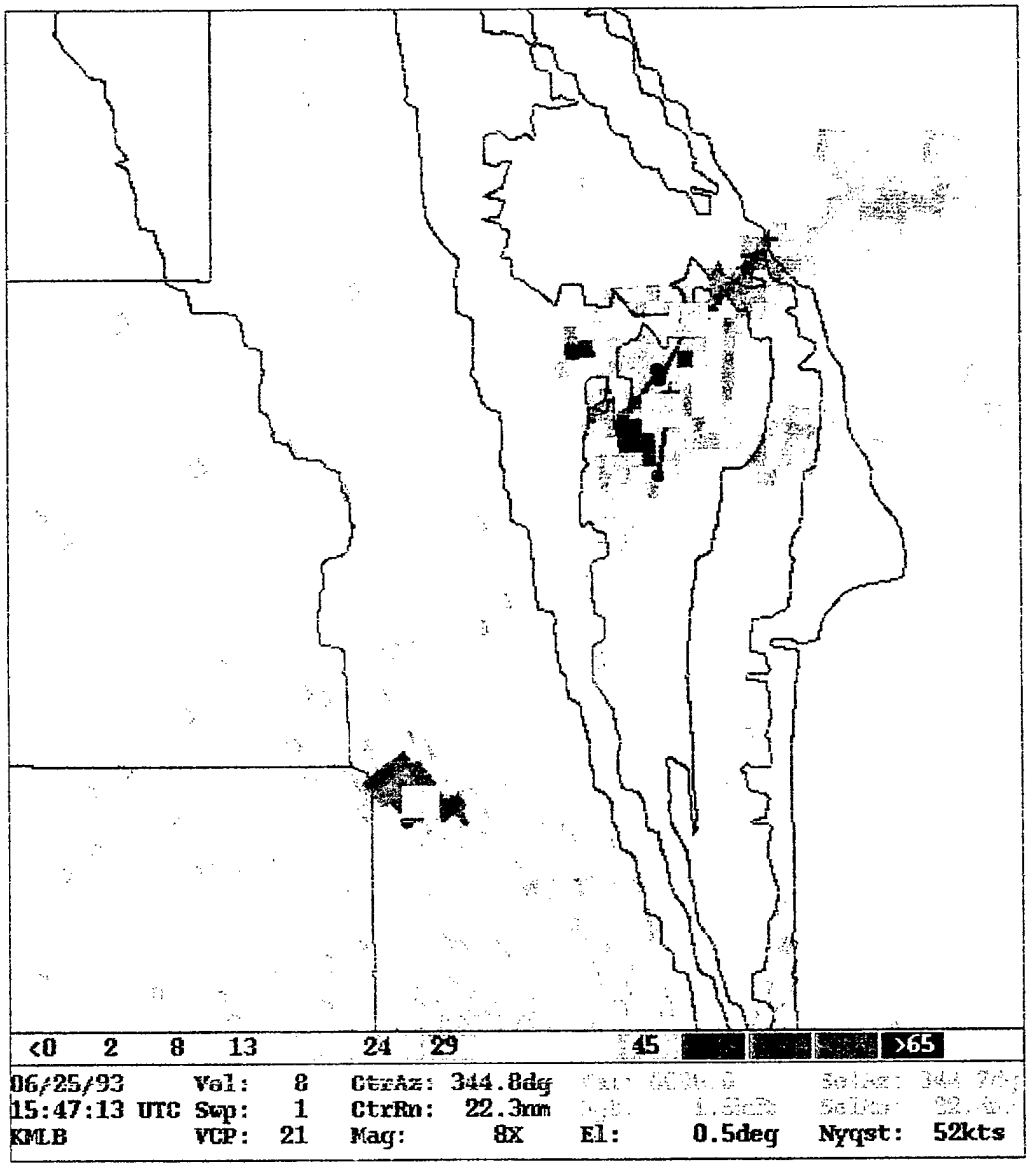

Figure 2.1. Example from the KMLB radar from 25 Jun 1993 of three cells identified by the SCIT algorithm. Cell 56 is a pulse cell, while cells 37 and 62 constitute a cluster and are not considered in this study.

is occurring over most of the domain and the issue of its "onset" is no longer a forecast concern.

2.2 Lightning Data

Lightning data for this study were obtained from the National Lightning Detection Network (NLDN). The NLDN network represents a network of 106 sensors located across the United States. The NLDN records and archives CG flash information with a detection efficiency of 80 to 90% (Idone et al. 1998a) and an average stroke location accuracy of 500 m (Idone et al. 1998b). The NLDN information for this study was obtained from the Air Force Combat Climatology Center in Asheville, NC. Individual flash information includes the time of the flash, in milliseconds, and the latitude and longitude, in thousandths of degrees.

NLDN flash information is mapped using the GEMPAK Analysis and Rendering Program (GARP) as described by the Unidata tutorial (Unidata web page 2000). Individual flashes are mapped using the latitude/longitude information from the NLDN archive and then overlaid on the radar data from WATADS. In this way, by using the radar to examine a developing cell, it could be determined when the first CG flash occurred. Once the first CG flash occurred, the LVIL properties of the cell for the preceding volume scans are be evaluated.

2.3 LVIL Calculation

The first step in the LVIL calculation is recording the maximum reflectivity at each individual elevation angle. Since the elevation angles on the WSR-88D cannot be positioned with respect to the storm between 0 and -20°C at 5-degree increments, there needs to be interpolation to these increments using the values that are available. For instance, figure 2.2 shows a sample reflectivity profile for a single volume scan. The temperature levels of interest are marked with a dashed line. The thickness of the individual temperature layers is determined from the morning sounding from Cape Canaveral (KXMR). The KXMR data were obtained from the Air Force Combat Climatology Center and consists of height, temperature, moisture and wind speed and direction for both the mandatory and significant levels. Linear interpolation is used between the reported levels and the temperature levels of interest. In order to find the reflectivity at the desired level, a cubic spline fit (Press et al., 1992, p. 107) is performed on these data. This cubic spline interpolation is done using MATLAB (Hanselman et al., 1996, p. 213), with the intention of providing a smooth fit across the data and providing a robust estimate of the maximum and minimum points.

Once the reflectivity at the five temperature levels is found, the LVIL can be computed for each individual layer. Greene (1972) first proposed Integrated Liquid-Water Content (VIL), equivalent to LVIL, as a tool for assessing the severe potential of storms. The current WSR-88D VIL algorithm (Federal Meteorological Handbook 11, 1991) also uses Greene's approach as defined by the equation:

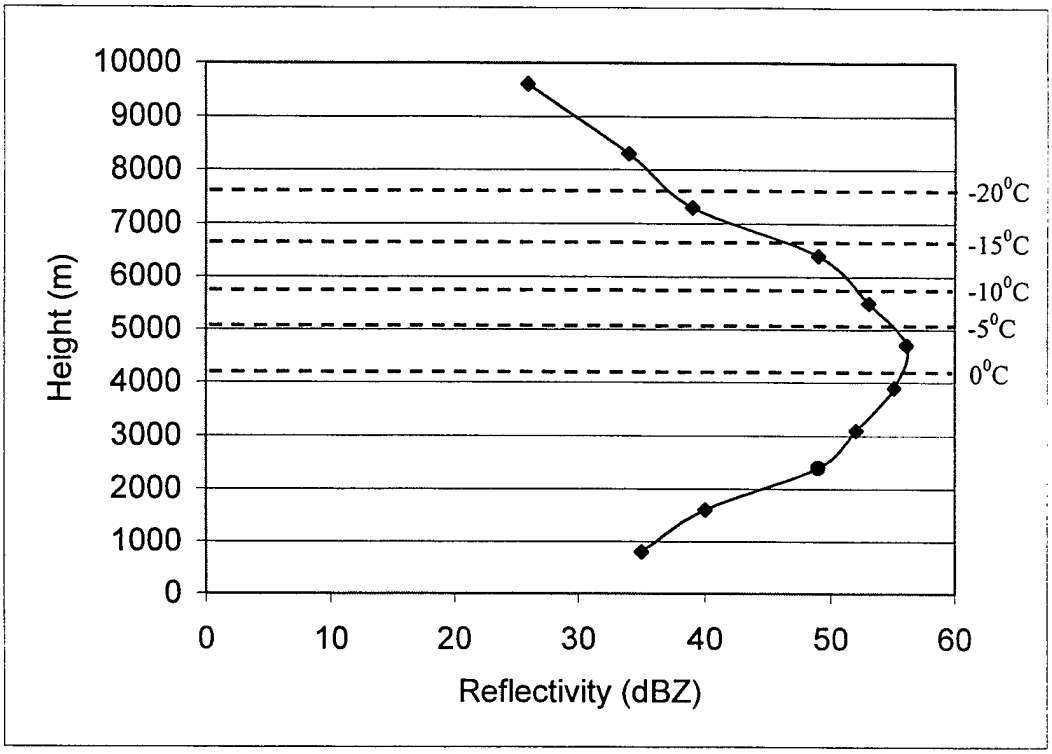

Figure 2.2. Sample reflectivity profile for one volume scan. Significant temperature levels, defined by the KXMR morning sounding, are shown. Note that there are no data points at the desired levels, necessitating the use of a cubic spline profile (solid curve) to smoothly find the points of interest for the LVIL calculation.

$$LVIL = \sum 3.44X10^{-6} [(Z_i + Z_{i+1})/2]^{4/7} dh \quad (1)$$

and has the units kilograms per square meter. Here, Z and Z_{i+1} are radar reflectivity values ($mm^6 m^{-3}$) at the lower and upper levels bounding the sampled layer and dh is the thickness of the layer in meters. The conversion from radar reflectivity in dBZ to the value of $mm^6 m^{-3}$ is given by the equation:

$$Z = 10^{(dBZ/10)} \quad (2)$$

The constant in (1) follows the assumption that the water drops in the layer obey the Marshall-Palmer (M-P) drop size distribution (Marshall and Palmer 1948). Although the cited distribution is highly variable, in summertime Florida convection, the M-P drop size distribution is widely used and so for consistency is used here.

Figure 2.3 is an example of the same reflectivity profile as in fig. 2.2. In fig. 2.3 the LVIL is obtained for the shaded sections that are the -10 to -15°C and -15 to -20°C layers. It can be seen from fig. 2.3 that larger reflectivities contribute to greater LVIL. The LVIL CG forecasting algorithm uses the Riemann integration approximation technique. In addition, the trapezoidal and Simpsons integration techniques were tested. However, because the reflectivity profile is smoothly varying with no significant changes in slope there is no significant improvement in the LVIL estimation with these two latter rules.

In all, four levels and their combinations are used to calculate LVIL for all volume scans up to and including the time of the first CG flash. Time t_o is given by the volume scan during which the first CG flash occurred. In addition, LVIL estimates for

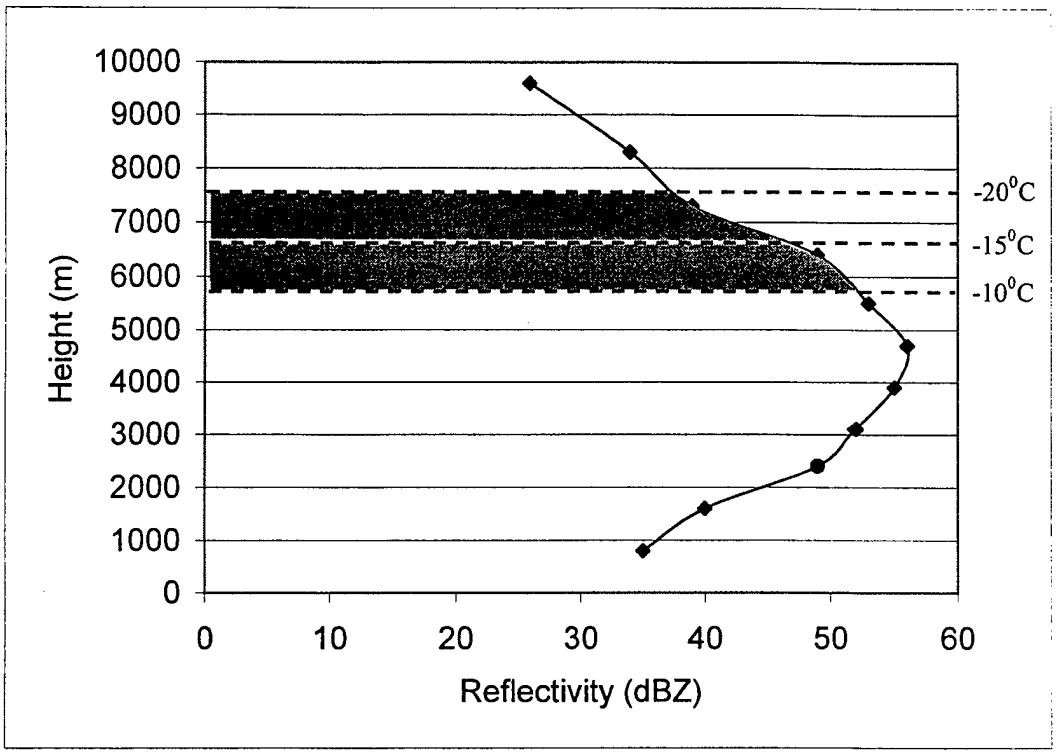

Figure 2.3. Same as figure 2.2 except that the -10 to -15°C and -15 to -20°C shaded sections represent the areas calculated by the LVIL algorithm.

the subsequent volume scan ($t_o + 1$) past the first CG flash are recorded but not included in the development of the algorithm.

2.4 Storm Statistics

For each storm there are three main statistics evaluated in order to develop a CG forecast algorithm. These statistics are generated from a 2X2 matrix as shown in figure 2.4 and the appendix (Wilks, 1995, p. 238). This matrix represents a yes/no observable outcome from a yes/no predictor. The predictors tested in this thesis are specific LVIL thresholds for individual layers and combinations of layers and are explained in detail in chapter 3. The first predictor is probability of detection (POD) as defined in Wilks (p. 240) by:

$$POD = a/(a + c) \tag{3}$$

The variables a and c are defined in figure 2.4. The second statistic is false alarm rate (FAR) as defined in Wilks (p. 241) by:

$$FAR = b/(a + b) \tag{4}$$

Another statistic evaluated on the LVIL database is the Kuipers skill score (KSS) as defined in Wilks (p. 249) by:

$$KSS = (ad - bc)/(a + c)(b + d) \tag{5}$$

The KSS represents skill over random forecasts that would receive a score of 0. Forecasts inferior to random forecasts receive negative scores while a perfect forecast receives a score of one.

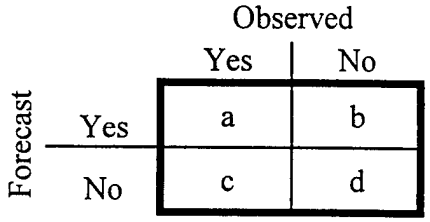

Figure 2.4. The 2X2 matrix used to provide measures of forecast skill in the formulation of the LVIL CG onset forecasting algorithm.

The final statistic computed on the LVIL database is the critical success index (CSI), also known as threat score. CSI is defined by Wilks (p. 240) by:

$$CSI = a/(a + b + c) \tag{6}$$

The KSS is preferable to the more widely used CSI because KSS includes the no/no (category d in fig. 2.4) forecasts in the computation (Doswell et al. 1990). Some forecast parameters have difficult *no* forecasts, and the CSI does not measure those forecast successes. Lightning forecasters, particularly during Florida convection, commonly are tempted to warn on any convective development. Lightning onset is difficult to predict; thus, a well-developed lightning algorithm attempts to increase the no/no and yes/yes hits and so maximize the KSS. In addition, CSI is not an unbiased measure of skill since the increase in frequency of an event artificially increases the estimate of forecast skill (Schaefer 1990). Therefore, KSS is deemed to be a more usable measure of forecast skill. Nevertheless, because CSI is easy to calculate and is a common statistic used to measure forecast skill it is included when showing results for this thesis; however, CSI will not be used in the development of the CG forecast algorithm.

Additionally, a weighted sum of LVIL (d-index) comprising the three main statistics is calculated for each layer and combination of layers. The d-index is defined by:

$$\text{d-index} = w_1\,\text{POD} + w_2\,\text{KSS} - w_3\,\text{FAR} \tag{7}$$

with POD, KSS and FAR being assigned the weights w_1, w_2 and w_3.

If the designated LVIL threshold criteria is met on one volume scan then the cell was considered to have a "yes" forecast. Many CG forecast algorithms, including the Pinder Principle and Gremillion's algorithm, require the forecast criteria to be satisfied for two successive volume scans before issuing a "yes" forecast. However, one half of the lightning-producing storms in this study existed for 10 minutes or less from cell identification to CG onset. In the case of these short-lived storms, the 5- to 6-minute scan strategy of the WSR-88D would not allow these storms to be forecasted with a stringent two-scan requirement in the algorithm. Thus, in order for a wide range of lightning-producing storms to be included in this study, only one volume scan is necessary for the issuance of a "yes" forecast. Also, the average leadtime, in minutes, is calculated and represents the time between when a CG forecast would be issued because the threshold criteria are met and the time of the first CG flash.

2.5 Storm Locations

For this study, 79 storms are analyzed over a five-year period (1993-97). Figure 2.5 shows east-central Florida and the locations of the 50 lightning-producing, pulse storms, while figure 2.6 shows the locations of the 29 non-lightning cases, termed hereafter as the null cases. All storms were located within 70 km of the KMLB radar to avoid analysis discrepancies with regard to beam broadening at great distances. Consistent with the typical diurnal trend, all storms occurred over land between 1000 and

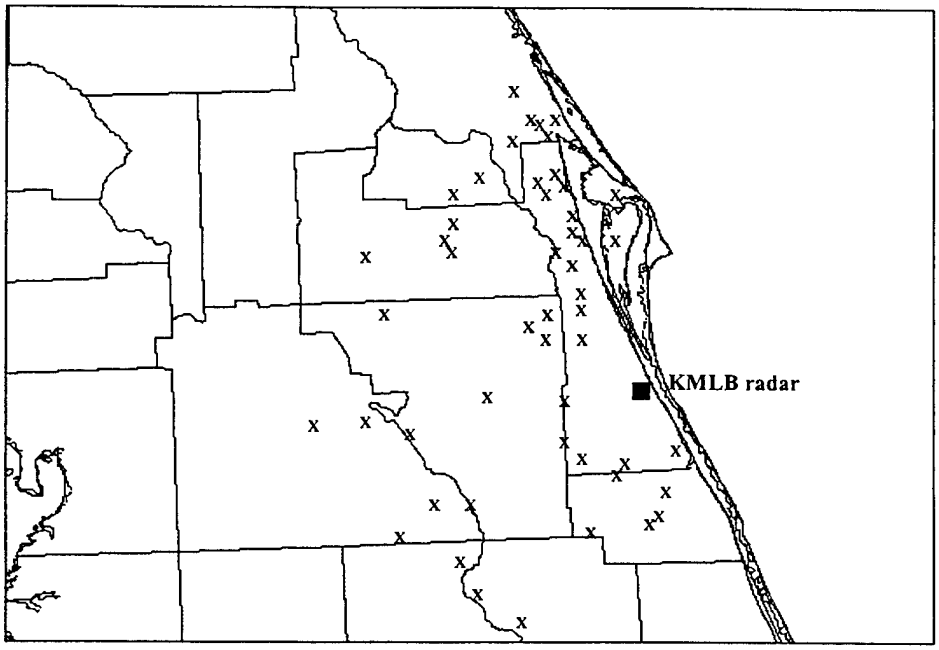

Figure 2.5. Locations, at the time of first CG flash, of the 50 lightning storms used in this study.

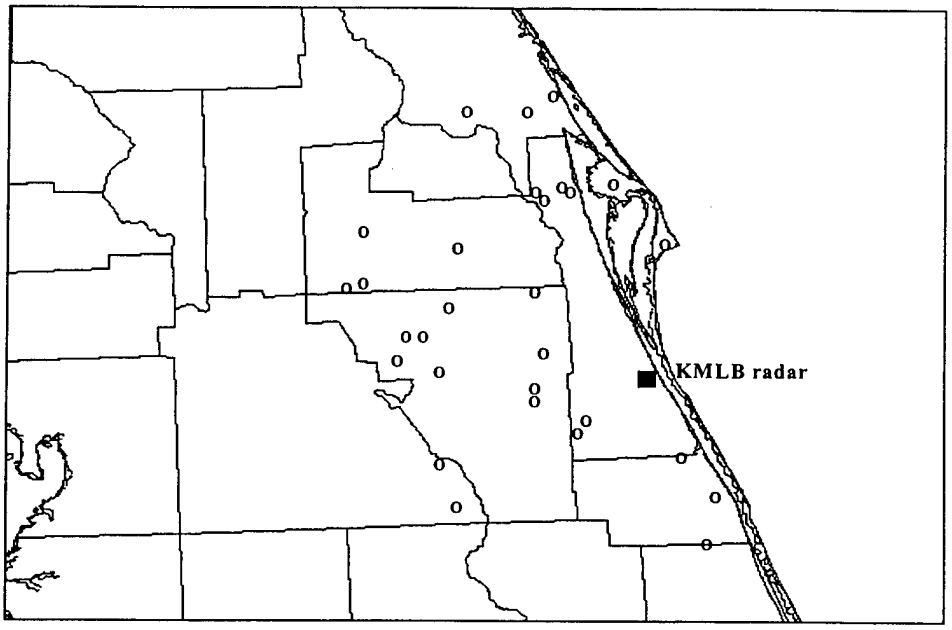

Figure 2.6. Locations of the 29 null-lightning storms used in this study.

1600 local time. Additionally, these locations agree with the findings of Hodanish (1997) with a concentration of storms occurring near the long-term maximum just west of KSC.

Chapter 3

RESULTS

This chapter presents a new theoretically based layered vertically integrated liquid (LVIL) cloud-ground (CG) forecast algorithm. This algorithm yields an improved probability of detection (POD) and Kuiper skill score (KSS) over those values given by the current methods used at the Kennedy Space Center (KSC).

3.1 Evaluation of Current Empirical Rules

There are presently two empirical rules used to forecast the onset of CG lightning at the KSC. The first rule, the "Pinder Principle," mandates that there be 45 dBZ reflectivity at the -10°C level. In addition, this 45 dBZ echo must extend at least 3000' above the -10°C level, which is roughly the -15°C level as given by a typical summertime sounding in Florida. The second rule in use at the KSC mandates that there be 4 mm of LVIL in the 0 to -20°C layer. This LVIL rule is experimental and provides the loose framework upon which the new algorithm is developed. Finally, Gremillion's (1998) study of pulse convection over east-central Florida between 1989 and 1996 shows that 30 dBZ at the -15°C level produces a POD of 96% and a false alarm rate (FAR) of 12%. Although Gremillion's result has not been incorporated operationally at the KSC, these favorable results suggest that this criterion should be tested on the same database used to develop the LVIL CG forecast algorithm.

The three current CG forecasting rules are evaluated using the 2X2 forecast matrix shown in figure 2.4. The results for the 45 dBZ at -10°C level rule (Pinder Principle) are shown in fig. 3.1. For the Pinder Principle, the POD is 72%, the FAR is 18%, the KSS is 44% and the CSI is 62%. Figure 3.2 shows the result of testing the LVIL database on Gremillion's threshold of 30 dBZ at the -15°C level. Gremillion's algorithm yields a POD of 100%, a FAR of 29%, a KSS of 31% and a CSI of 71%. Although the POD agrees with the earlier results of Gremillion, the FAR is considerably higher, and the KSS considerably lower, than the result attained using the Pinder Principle. Finally, the new, experimental LVIL algorithm of 4 mm in the 0 and –20°C layer yields a POD of 92%, a FAR of 29%, a KSS of 26% and a CSI of 67% (fig. 3.3). Clearly, the experimental LVIL algorithm performed the worst of the three rules with the highest FAR and lowest KSS, despite having a high POD. Thus, it is clear that a new LVIL algorithm is needed that incorporates new parameters that yield results exceeding the performance of the Pinder Principle – the best performer of the three in evaluating a forecast of the onset of CG lightning.

3.2 Lightning Characteristics

In order to improve the experimental LVIL algorithm currently in use at the KSC, there must be a refinement of both the threshold applied and the temperature levels used. Figure 3.4 shows the average dBZ profile in the 0 to -20°C layer for the lightning and null lightning cases studied here. Averaging the reflectivity in the 0 to -20°C layer at

>45 dBZ above the -10°C level for 3000'			
		observed	
		yes	no
forecast	yes	36	8
	no	14	21
	POD	72	
	FAR	18	
	KSS	44	
	CSI	62	

Figure 3.1. The 2X2 forecast matrix results for the Pinder Principle CG forecasting rule currently in operational use at the KSC.

30 dBZ at the -15°C level			
		observed	
		yes	no
forecast	yes	50	20
	no	0	9
	POD	100	
	FAR	29	
	KSS	31	
	CSI	71	

Figure 3.2. The 2X2 forecast matrix for 30 dBZ at -15°C threshold (Gremillion 1998).

0 to -20°C layer: 4.0mm threshold			
		observed	
		yes	no
forecast	yes	46	19
	no	4	10
	POD	92	
	FAR	29	
	KSS	26	
	CSI	67	

Figure 3.3. The 2X2 forecast matrix for the 4 mm threshold between the 0 and the -20°C levels (KSC experimental LVIL).

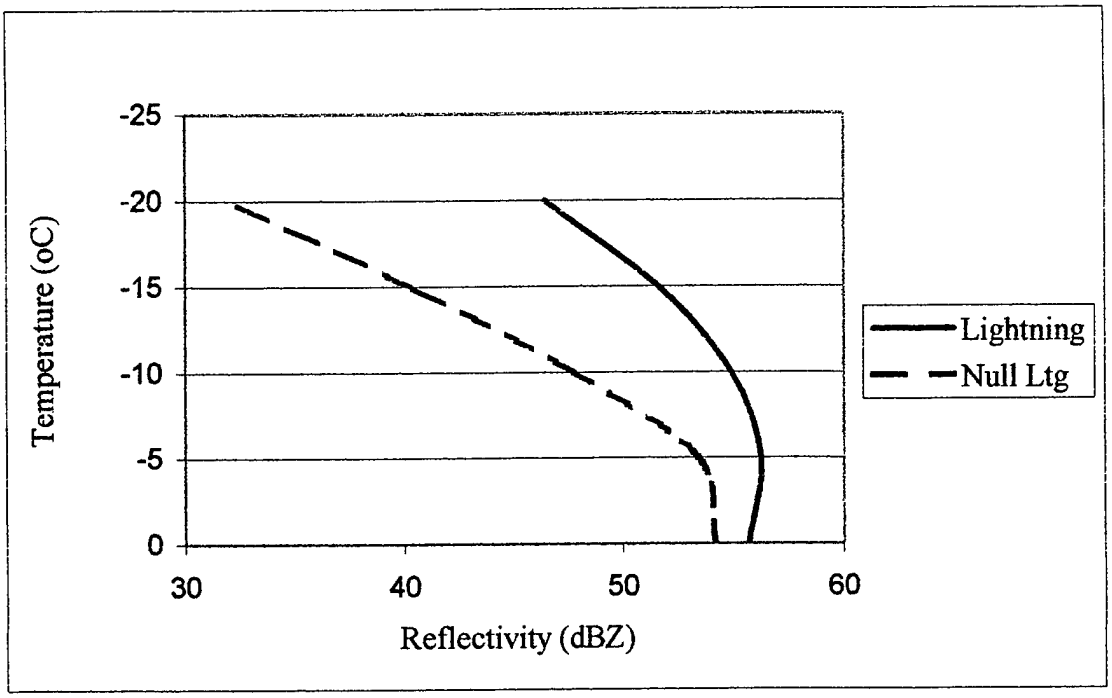

Figure 3.4. Average reflectivity profile for the 50 lightning and 29 null lightning cases used in the LVIL database. This profile provides the motivation for exploring the storm LVIL characteristics in the -10 to -20°C layer. The average reflectivity is derived from either the time of first CG occurrence (lightning cases) or the time of highest 0 to -20°C LVIL achieved (null cases).

the time of the first CG flash creates the profile for the 50 lightning cases (solid curve). The profile for the null lightning cases (dashed curve) is an average of 29 cases when the LVIL in the 0 to -20°C layer is the highest. Generally, the highest LVIL achieved in the null cases occurs four volume scans (approximately 20 minutes) after the SCIT algorithm first detects a cell (refer to section 2.1 for SCIT). Similarly, the time of first CG flash occurs about four volume scans after the SCIT algorithm identifies the cell.

Inspection of fig. 3.4 shows that the reflectivity in the 0 to -10°C layer, and in particular in the 0 to -5°C layer, is within a few dBZ of one another for both the lightning and null cases. The difference in the dBZ profile is most marked in -10 to -20°C layer. At -10°C the difference is 7 dBZ while the difference at -20°C is 14 dBZ. Thus, it appears that there is value to be gained by isolating the -10 to -20°C layer when developing a LVIL CG forecast algorithm. Moreover, this -10 to -20°C layer has been shown to be the primary layer where charge generation and lightning initiation occurs (Dye 1986 and Ziegler 1986). This -10 to -20°C layer is broken into two 5°C deep layers with properties of both and their combination evaluated in the next section. The goal of a new algorithm is to outperform the existing CG forecasting rules at the KSC, notably the Pinder Principle.

3.3 New LVIL Algorithm

First, individual thresholds in 0.5 mm increments are tested on all 5°C deep layers within the 0 to -20°C layer. One immediate problem with this one-layer approach is the

unavoidable compromise between achieving a high POD and KSS while limiting FAR. In addition, the statistics for one layer can be similar to those of another layer, making the choice of which bounding levels to incorporate in an algorithm difficult. For instance, the threshold of 0.5 mm between -10 and -15°C (shown in fig. 3.5) achieves a POD of 82%, a FAR of 16%, a KSS of 54% and a CSI of 68%. Meanwhile, a threshold of 1.5 mm between the -15 and -20°C level (shown in fig. 3.6) achieves similar results. The criteria for these two levels produce the best scores among the many thresholds and levels tested. As a stand-alone forecast tool, the results in figs. 3.5 and 3.6 achieve a lower POD than either Gremillion's threshold or the experimental LVIL rule (4 mm in the 0 to -20°C layer).

An immediate question arises as to whether the lower POD of figs. 3.5 and 3.6 is acceptable in return for a higher KSS and lower FAR. Mr. William Roeder, Chief Staff Meteorologist at the KSC, notes that in the interest of personnel safety and ground operations at the KSC, it is desirable to have the highest POD possible while still maintaining "reasonably" high KSS and "reasonably" low FAR (Roeder, Personal Communication, 2000). Thus, the challenge in choosing an appropriate threshold to meet the operational needs of the KSC is clear. At the very least, the POD achieved in fig. 3.5 and 3.6 is too low to be acceptable when compared with Gremillion's threshold and the experimental LVIL.

What has not yet been incorporated into the threshold criterion is the vertical structure of the storm as seen in fig. 3.4. A first step in incorporating the vertical

-10 to -15°C layer: 1.5 mm threshold			
		observed	
		yes	no
forecast	yes	39	7
	no	11	22
	POD	78	
	FAR	15	
	KSS	54	
	CSI	68	

Figure 3.5. The 2X2 forecast matrix for the 1.5 mm threshold between the -10 and -15°C levels.

-15 to -20°C layer: 0.5 mm threshold			
		observed	
		yes	no
forecast	yes	41	8
	no	9	21
	POD	82	
	FAR	16	
	KSS	54	
	CSI	71	

Figure 3.6. The 2X2 forecast matrix for the 0.5 mm threshold between the -15 and -20°C levels.

structure of the storm is to require two thresholds to be met simultaneously in the two layers used in figs. 3.5 and 3.6. In order to find the best pair (x,y) of thresholds for the -10 to -15°C and the -15 to -20°C layers, all combinations are evaluated using POD, FAR and KSS. An issue then arises as to which single parameter best measures forecast skill.

The highest POD is in the lower left portion of fig. 3.7 and is a maximum at the point (0.1 mm/0.1 mm), which is 0.1 mm for both the -10 to -15°C and -15 to -20°C layers. Similarly, the highest FAR values also occur in the lower left portion of fig. 3.8. Clearly, a high POD and a low FAR cannot both be achieved simultaneously when using this two-layer approach. Furthermore, the KSS (shown in figure 3.9) is maximized around the threshold pair (1.5 mm/0.5 mm). Thus, since POD, KSS and FAR are maximized in different regions of figs. 3.7 – 3.9 a question arises as to what threshold pair is the POD operationally useful with an acceptable KSS and FAR.

Evaluating POD, FAR and KSS together via their weighted sum (d-index in section 2.4) can better produce a threshold than can a single-parameter approach. The results of this d-index are shown in figure 3.10 for the weights $w_1 = w_2 = w_3 = 1$. The highest weighted sum in fig. 3.10 is centered on the threshold pair (0.5 mm/0.25 mm). The POD for this threshold pair (0.5 mm/0.25 mm) is 96%, the FAR is 21% and the KSS is 51%.

In addition to assigning POD, KSS and FAR equal weights, the d-index was evaluated by applying several different weighting schemes. Mr. William Roeder remarked, from an operational perspective, that POD is the most significant statistic

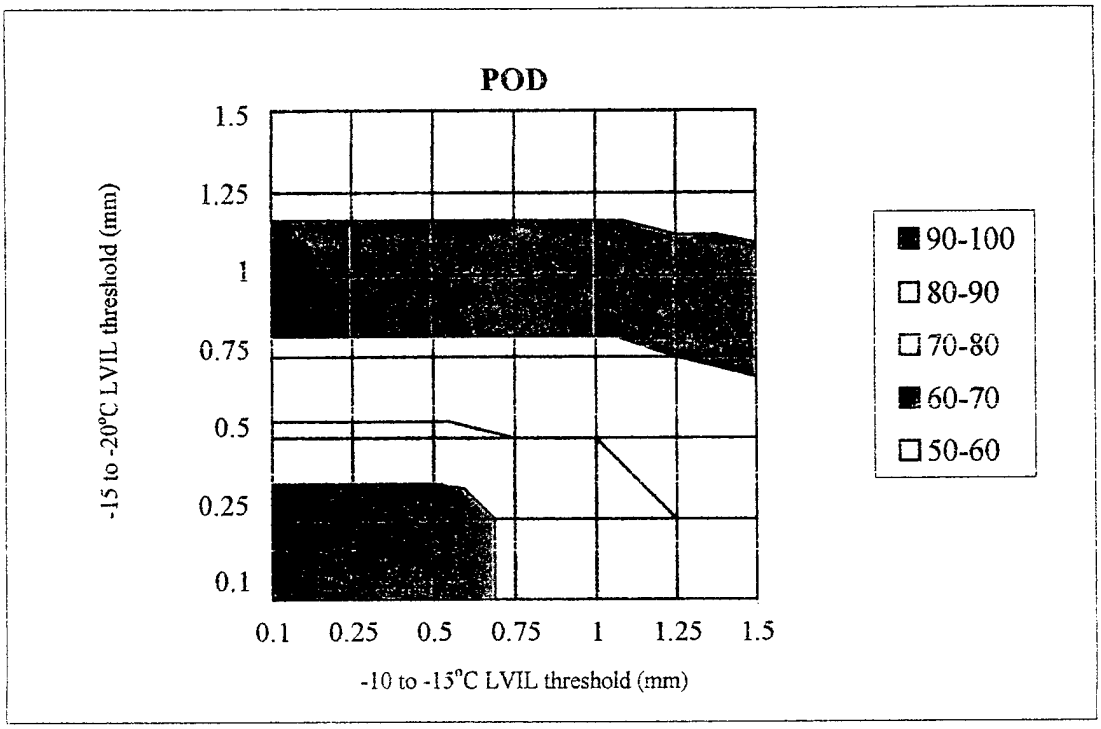

Figure 3.7. POD for combinations of thresholds for the -10 to -15°C layer and the -15 to -20°C layer.

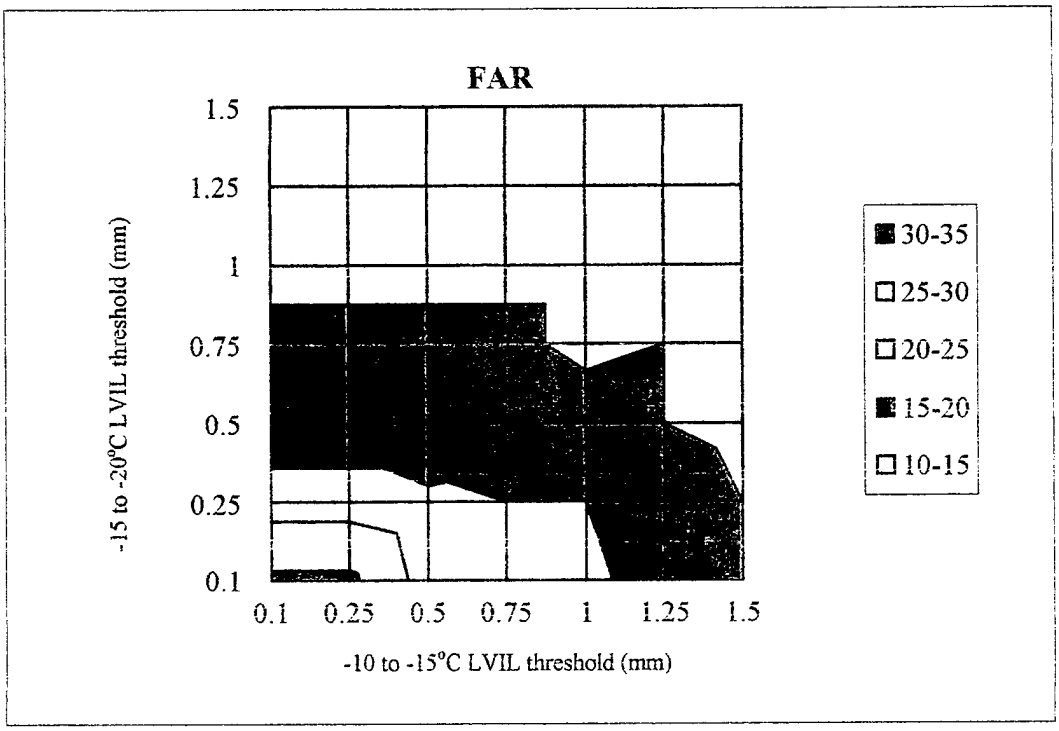

Figure 3.8. Same as fig. 3.7 except for FAR.

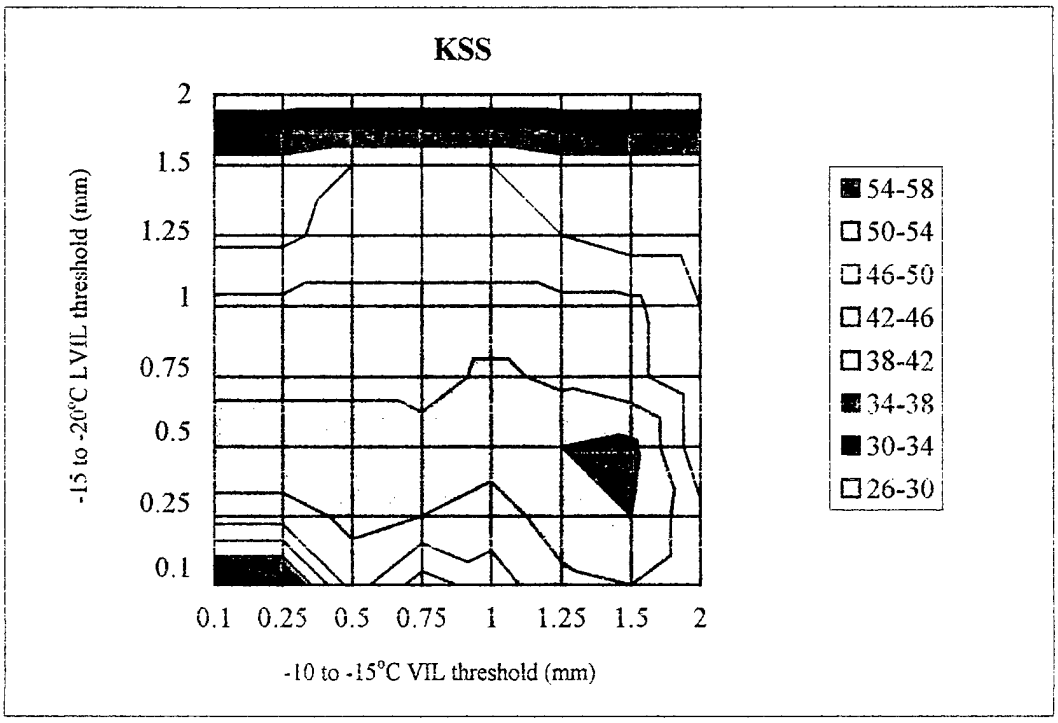

Figure 3.9. Same as fig. 3.7 except for KSS.

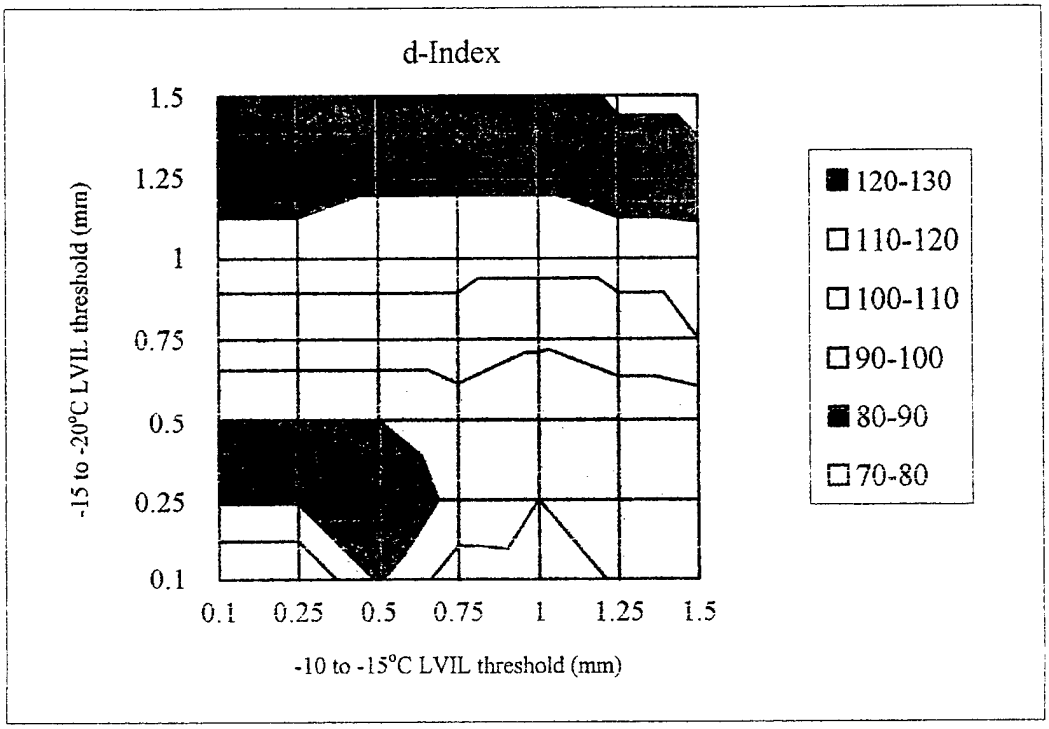

Figure 3.10. Same as fig. 3.7 except for weighted sum of POD, FAR and KSS with weights $w_1 = w_2 = w_3 = 1$. The threshold pair 0.5 mm/0.25 mm represents the best CG forecast skill value (126).

while KSS and FAR is less significant. Therefore, the d-index is changed to define weights as above, for $w_1 = 3$, $w_2 = 2$ and $w_3 = 1$ and $w_1 = 2$, $w_2 = 1$ and $w_3 = 1$ respectively. The use of the greatest weighting for POD results from William Roeder's noting that detection is most critical when making personnel safety decisions. In both weighting schemes the threshold pair (0.5 mm/0.25 mm) gives the highest weighted sum of all threshold pairs tested (figs. 3.11 and 3.12), similar to the equal weights used in fig. 3.10 for the d-index. Thus, the agreement across several weight schemes strengthens the confidence in recommending the aforementioned threshold pair that must be met for a CG forecast to be issued.

Only by combining the skill statistics into a single parameter d does a definite threshold pair arise that yields a high POD and KSS but a low FAR. Moreover, the threshold pair (0.5 mm/0.25 mm) best accomplishes the aforementioned operational needs of the KSC as summarized by Roeder (2000). The individual 2X2 forecast matrices for all thresholds are presented in the appendix.

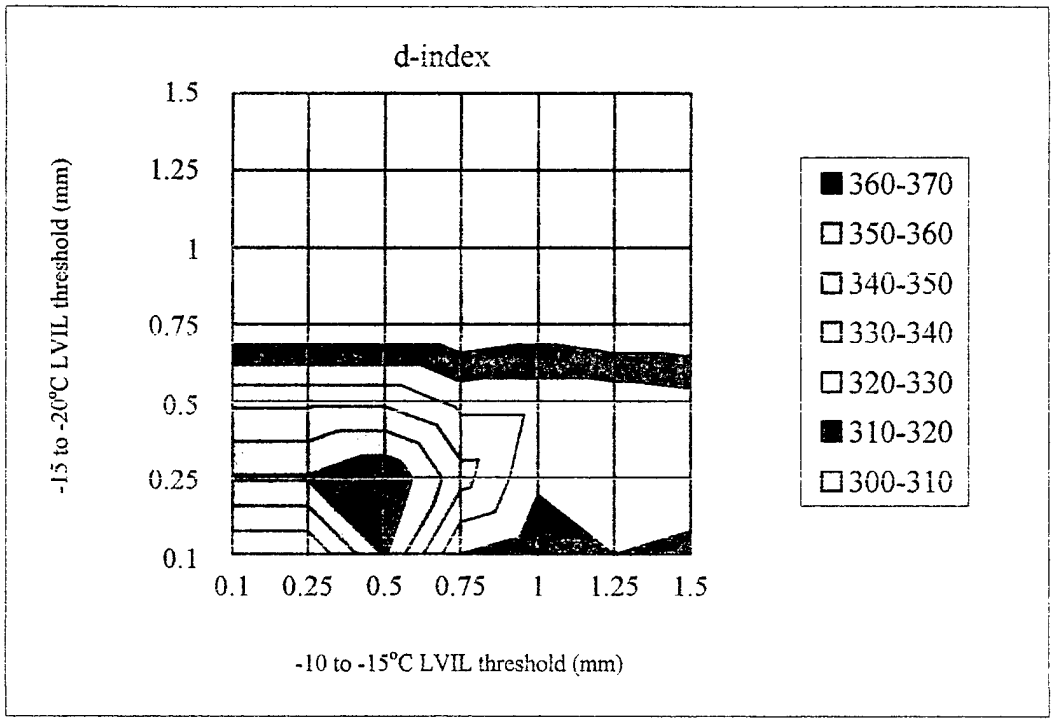

Figure 3.11. Same as fig. 3.10 except for weights $w_1 = 3$, $w_2 = 2$ and $w_3 = 1$. The 0.5 mm/0.25 mm point still represents the best CG forecast skill.

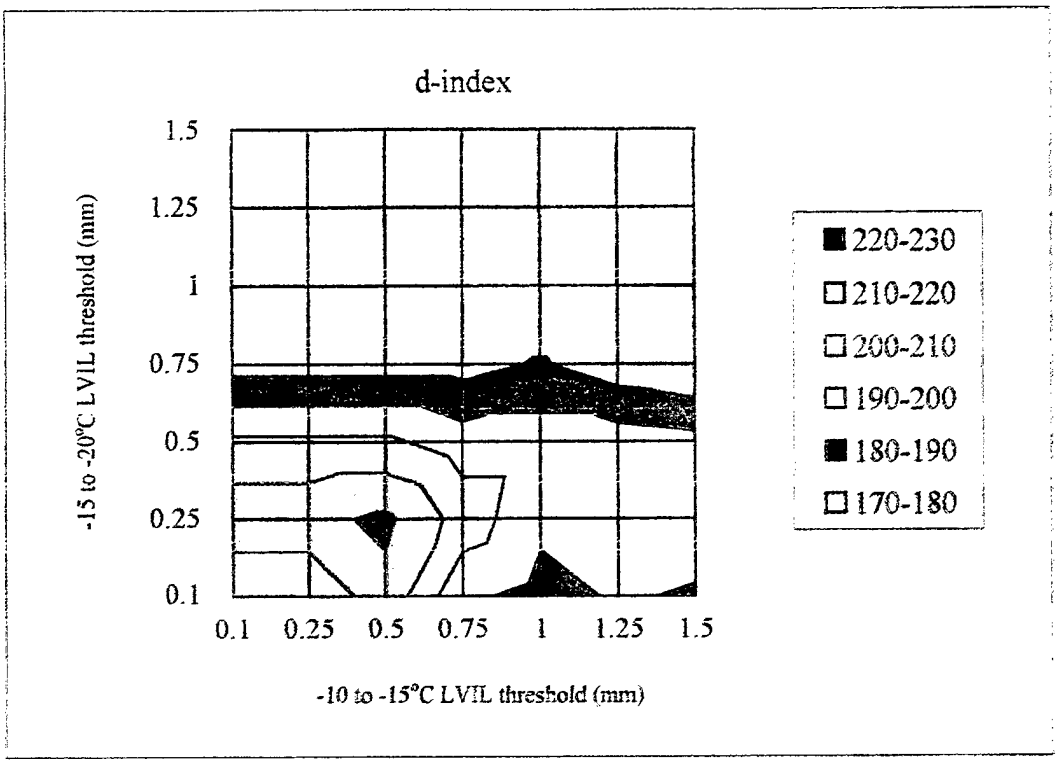

Figure 3.12. Same as fig. 3.10 except for weights $w_1 = 2$, $w_2 = 1$ and $w_3 = 1$. The 0.5 mm/0.25 mm point still represents the best CG forecast skill.

Chapter 4

CONCLUSION

Accurate forecasting of cloud-ground (CG) lightning onset at the Kennedy Space Center (KSC), Florida is critical for both resource protection and personnel safety, but represents a difficult problem. Current methods for predicting CG lightning onset rely on radar analyses that require a reflectivity threshold to be exceeded at a specific temperature level. Although the requisite temperature level used in lightning forecasting lies within the critical region of convection for lightning initiation (-10 to -20°C), current methods of prediction do not employ a complete description of the storm structure. This thesis hypothesizes that diagnosing the storm structure within the -10 to -20°C layer is a key element in forecasting lightning onset. This structure can readily be described by the variation of liquid water content in the -10 to -20°C layer. Recent software advances with the WSR-74C radar at the KSC have enabled forecasters to examine the water content of a storm in real-time using layered vertically integrated liquid (LVIL). Reflectivity, a readily available radar product, is used to estimate LVIL. This thesis examines the vertical structure of a storm by computing LVIL within two layers in the supercooled region (in the -10 to -15°C and -15 to -20°C layers). LVIL values, for both layers, described together as a threshold pair, quantify the minimum vertical structure required for lightning onset. Specifically, LVIL amounts of 0.5 mm in the -10 to -15°C layer coinciding with amounts of 0.25 mm in the -15 to -20°C layer indicates that lightning is imminent with a probability of detection of (POD) of 96%, a false alarm rate (FAR) of

21% and a Kuipers skill score (KSS) of 51%. This two-layer approach is superior to one-parameter methods currently in use at the KSC.

Meeting the operational needs of the KSC must be paramount when developing any CG forecast algorithm. A successful algorithm utilizes the weighted sum of POD, KSS and FAR to find the threshold pair with the highest overall skill. Two-layer algorithms evaluated using only one statistic at a time produce conflicting results, as POD, KSS and FAR cannot be optimized simultaneously. Often a lower FAR is achieved at the expense of a lower POD and vice versa. Operationally, this scenario creates ambiguity in choosing which layer and which thresholds are "optimal" and so is unacceptable. Thus, a weighting scheme that eliminates ambiguity between the three major statistics is necessary. Because detection is the critical element for personnel safety, the LVIL CG forecast algorithm is optimized by weighting POD the highest, followed by KSS and FAR. The resulting threshold pair (0.5 mm/0.25 mm) is given by several weighting schemes that follow this order of importance and so provides an operationally significant forecast parameter that best meets the needs of the KSC. Despite this work being a significant first step in the use of LVIL to forecast the onset of CG lightning, there remain many areas for improvement.

Ideally, a forecaster would have two successive volume scans on which to base a CG forecast. The current LVIL CG forecast technique must warn on only one satisfaction of the threshold pair criteria because the 5- to 6-minute volume scan strategy of the WSR-88D does not allow adequate sampling of rapidly developing storms. In

contrast, the WSR-74C scans twice as fast allowing the forecaster to require the criteria to be satisfied on two successive volume scans before issuing a CG forecast. This approach should lead to improved forecast skill.

The CG forecast algorithm is developed using WSR-88D data. However, the coarse vertical and temporal resolution of this radar is surpassed by the WSR-74C, the primary radar at the KSC. The better vertical resolution of the WSR-74C may help refine the LVIL threshold in the -10 to -20°C layer. A more significant benefit of using the WSR-74C is the more frequent, 2.5-minute volume scan strategy that is twice as frequent as the 5- to 6-minute volume scan strategy of the WSR-88D. The average leadtime for all layers and thresholds ranges between 7 and 12 minutes, as listed in the appendix. Because this range in leadtimes is less than the 5-6 minute volume scan of the WSR-88D, this variation in leadtimes is not meaningful. Testing the result of this thesis using WSR-74C radar data may help make useful the 7- to 12-minute average leadtime found both in this work and in earlier studies. Notwithstanding, the leadtime issue may still be constrained by the fact that many storms (~50% in this database) initiate lightning within 10 minutes of the first reflectivity detection.

Another area for improvement is to increase the size of the storm database to include non-pulse convection. Lightning originating from lines and clusters of convection, while a more intractable problem from a cell identification standpoint, accounts for much lighting activity in Florida. This thesis develops a CG forecast algorithm using the simplest type of storm that could be identified on radar. As merging

storms, clusters and lines of convection often produce a significant lightning threat; an algorithm incorporating this category of convection would prove beneficial. Perhaps different types of convection require different thresholds that must be determined if CG lightning from all types of convection is to be forecast.

Because NLDN data for an entire lifetime of a storm are available, a question is whether the LVIL values and their trend prior to CG onset could be used to predict the amount and duration of lightning during the entire storm. The present work is only concerned with CG lightning onset, and so the issue of the total amount of lightning was not examined. A prediction of lightning amount and duration might be operationally significant in the sense that it would allow personnel to plan for a "lightning period." A prediction of the duration and amount of lightning could give operators an idea of how much time might be lost to lightning activity.

Another natural extension of the study would be to examine the problem of predicting cloud-to-cloud (CC) lightning onset. A CC lightning forecast would benefit the KSC in preparing for space launches for which the CC lightning threat is a much greater concern than is CG lightning.

Finally, incorporating a measure of the electric (E) field would enable forecasters to add an important parameter independent of radar. Use of the KSC field mill network with the LVIL CG forecast algorithm might provide the next significant step in lightning forecasting. The addition of the vertical structure of reflectivity in the new CG forecast algorithm presented here makes use of an undeveloped radar technique. Important future

advancements are more likely, however, through the incorporation of parameters that are independent of radar reflectivity. Perhaps both E-field measurements and dual-polarization radar will play a lead role in improving lightning forecasting techniques.

Although there are many areas requiring further study, this research represents an important step in improving the forecasts of the onset of CG lightning. This work introduces a new approach to the problem by using LVIL to demonstrate the importance of the vertical structure of reflectivity. The KSC should find these results operationally beneficial and use them as a springboard to new ideas and future improvements.

Appendix

2X2 forecast matrices used in the development of the two-layer LVIL CG forecast algorithm. POD - Probability of Detection, FAR - False Alarm Rate, KSS - Kuipers Skill Score, LT - Leadtime

-10 to -15: 0.1mm; -15 to -20C: 0.1mm

		observed: yes	observed: no
forecast	yes	50	20
	no	0	9

POD	100
FAR	29
KSS	31
CSI	71
Avg LT (min)	12

-10 to -15: 0.1mm; -15 to -20C: 0.25mm

		observed: yes	observed: no
forecast	yes	48	14
	no	2	15

POD	96
FAR	23
KSS	48
CSI	75
Avg LT (min)	10

-10 to -15: 0.25mm; -15 to -20C: 0.1mm

		observed: yes	observed: no
forecast	yes	50	20
	no	0	9

POD	100
FAR	29
KSS	31
CSI	71
Avg LT (min)	12

-10 to -15: 0.25mm; -15 to -20C: 0.25mm

		observed: yes	observed: no
forecast	yes	48	14
	no	2	15

POD	96
FAR	23
KSS	48
CSI	75
Avg LT (min)	9.6

-10 to -15: 0.5mm; -15 to -20C: 0.1mm

		observed: yes	observed: no
forecast	yes	48	14
	no	2	15

POD	96
FAR	23
KSS	48
CSI	75
Avg LT (min)	10

-10 to -15: 0.5mm; -15 to -20C: 0.25mm

		observed: yes	observed: no
forecast	yes	48	13
	no	2	16

POD	96
FAR	21
KSS	51
CSI	76
Avg LT (min)	9.6

-10 to -15: 0.75mm; -15 to -20C: 0.1mm

		observed: yes	observed: no
forecast	yes	44	14
	no	6	15

POD	88
FAR	24
KSS	40
CSI	69
Avg LT (min)	9.2

-10 to -15: 0.75mm; -15 to -20C: 0.25mm

		observed: yes	observed: no
forecast	yes	44	11
	no	6	18

POD	88
FAR	20
KSS	50
CSI	72
Avg LT (min)	9.4

Appendix

2X2 forecast matrices used in the development of the two-layer LVIL CG forecast algorithm. POD - Probability of Detection, FAR - False Alarm Rate, KSS - Kuipers Skill Score, LT - Leadtime

-10 to -15: 1.0mm; -15 to -20C: 0.1mm

		observed	
		yes	no
forecast	yes	41	11
	no	9	18

POD	82
FAR	21
KSS	44
CSI	67
Avg LT (min)	9

-10 to -15: 1.0mm; -15 to -20C: 0.25mm

		observed	
		yes	no
forecast	yes	41	10
	no	9	19

POD	82
FAR	20
KSS	48
CSI	68
Avg LT (min)	9

-10 to -15: 1.25mm; -15 to -20C: 0.1mm

		observed	
		yes	no
forecast	yes	40	9
	no	10	20

POD	80
FAR	18
KSS	49
CSI	68
Avg LT (min)	8.8

-10 to -15: 1.25mm; -15 to -20C: 0.25mm

		observed	
		yes	no
forecast	yes	40	8
	no	10	21

POD	80
FAR	17
KSS	52
CSI	69
Avg LT (min)	8.8

-10 to -15: 1.5mm; -15 to -20C: 0.1mm

		observed	
		yes	no
forecast	yes	39	8
	no	11	21

POD	78
FAR	17
CSI	67
KSS	50
Avg LT (min)	8.6

-10 to -15: 1.5mm; -15 to -20C: 0.25mm

		observed	
		yes	no
forecast	yes	39	7
	no	11	22

POD	78
FAR	15
CSI	68
KSS	54
Avg LT (min)	8.6

Appendix

2X2 forecast matrices used in the development of the two-layer LVIL CG forecast algorithm. POD - Probability of Detection, FAR - False Alarm Rate, KSS - Kuipers Skill Score, LT - Leadtime

-10 to -15: 0.1mm; -15 to -20C: 0.5mm

		observed	
		yes	no
forecast	yes	41	8
	no	9	21

POD	82
FAR	16
KSS	54
CSI	71
Avg LT (min)	9

-10 to -15: 0.1mm; -15 to -20C: 0.75mm

		observed	
		yes	no
forecast	yes	36	7
	no	14	22

POD	72
FAR	16
KSS	48
CSI	63
Avg LT (min)	7.9

-10 to -15: 0.25mm; -15 to -20C: 0.5mm

		observed	
		yes	no
forecast	yes	41	8
	no	9	21

POD	82
FAR	16
KSS	54
CSI	71
Avg LT (min)	9

-10 to -15: 0.25mm; -15 to -20C: 0.75mm

		observed	
		yes	no
forecast	yes	36	7
	no	14	22

POD	72
FAR	16
KSS	48
CSI	63
Avg LT (min)	7.9

-10 to -15: 0.5mm; -15 to -20C: 0.5mm

		observed	
		yes	no
forecast	yes	41	8
	no	9	21

POD	82
FAR	16
KSS	54
CSI	71
Avg LT (min)	9

-10 to -15: 0.5mm; -15 to -20C: 0.75mm

		observed	
		yes	no
forecast	yes	36	7
	no	14	22

POD	72
FAR	16
KSS	48
CSI	63
Avg LT (min)	7.9

-10 to -15: 0.75mm; -15 to -20C: 0.5mm

		observed	
		yes	no
forecast	yes	40	8
	no	10	21

POD	80
FAR	17
KSS	52
CSI	69
Avg LT (min)	9

-10 to -15: 0.75mm; -15 to -20C: 0.75mm

		observed	
		yes	no
forecast	yes	36	7
	no	14	22

POD	72
FAR	16
KSS	48
CSI	63
Avg LT (min)	7.9

Appendix

2X2 forecast matrices used in the development of the two-layer LVIL CG forecast algorithm. POD - Probability of Detection, FAR - False Alarm Rate, KSS - Kuipers Skill Score, LT - Leadtime

-10 to -15: 1.0mm; -15 to -20C: 0.5mm

		observed	
		yes	no
forecast	yes	40	8
	no	10	21

POD	80	
FAR	17	
KSS	52	
CSI	69	
Avg LT (min)		9

-10 to -15: 1.0mm; -15 to -20C: 0.75mm

		observed	
		yes	no
forecast	yes	36	6
	no	14	23

POD	72	
FAR	14	
KSS	51	
CSI	64	
Avg LT (min)		7.9

-10 to -15: 1.25m; -15 to -20C: 0.5mm

		observed	
		yes	no
forecast	yes	39	7
	no	11	22

POD	78.00	
FAR	15.22	
KSS	53.86	
CSI	68.42	
Avg LT (min)		8.6

-10 to -15: 1.25mm; -15 to -20C: 0.75mm

		observed	
		yes	no
forecast	yes	35	6
	no	15	23

POD	70	
FAR	15	
KSS	49	
CSI	63	
Avg LT (min)		7.9

-10 to -15: 1.5m; -15 to -20C: 0.5mm

		observed	
		yes	no
forecast	yes	38	6
	no	12	23

POD	76	
FAR	14	
CSI	68	
KSS	55	
Avg LT (min)		8.3

-10 to -15: 1.5mm; -15 to -20C: 0.75mm

		observed	
		yes	no
forecast	yes	34	6
	no	16	23

POD	68	
FAR	15	
CSI	61	
KSS	47	
Avg LT (min)		7.9

Appendix

2X2 forecast matrices used in the development of the two-layer LVIL CG forecast algorithm. POD - Probability of Detection, FAR - False Alarm Rate, KSS - Kuipers Skill Score, LT - Leadtime

-10 to -15: 0.1mm; -15 to -20C: 1.0mm

		observed	
		yes	no
forecast	yes	32	5
	no	18	24

POD	64	
FAR	14	
KSS	47	
CSI	58	
Avg LT (min)		7.3

-10 to -15: 0.1mm; -15 to -20C: 1.25mm

		observed	
		yes	no
forecast	yes	29	5
	no	21	24

POD	58	
FAR	15	
KSS	41	
CSI	53	
Avg LT (min)		7

-10 to -15: 0.25mm; -15 to -20C: 1.0mm

		observed	
		yes	no
forecast	yes	32	5
	no	18	24

POD	64	
FAR	14	
KSS	47	
CSI	58	
Avg LT (min)		7.3

-10 to -15: 0.25mm; -15 to -20C: 1.25mm

		observed	
		yes	no
forecast	yes	29	5
	no	21	24

POD	58	
FAR	15	
KSS	41	
CSI	53	
Avg LT (min)		7

-10 to -15: 0.5mm; -15 to -20C: 1.0mm

		observed	
		yes	no
forecast	yes	32	5
	no	18	24

POD	64	
FAR	14	
KSS	47	
CSI	58	
Avg LT (min)		7.3

-10 to -15: 0.5mm; -15 to -20C: 1.25mm

		observed	
		yes	no
forecast	yes	29	4
	no	21	25

POD	58	
FAR	12	
KSS	44	
CSI	54	
Avg LT (min)		7

-10 to -15: 0.75mm; -15 to -20C: 1.0mm

		observed	
		yes	no
forecast	yes	32	5
	no	18	24

POD	64	
FAR	14	
KSS	47	
CSI	58	
Avg LT (min)		7.3

-10 to -15: 0.75mm; -15 to -20C: 1.25mm

		observed	
		yes	no
forecast	yes	29	4
	no	21	25

POD	58	
FAR	12	
KSS	44	
CSI	54	
Avg LT (min)		7

Appendix

2X2 forecast matrices used in the development of the two-layer LVIL CG forecast algorithm. POD - Probability of Detection, FAR - False Alarm Rate, KSS - Kuipers Skill Score, LT - Leadtime

-10 to -15: 1.0mm; -15 to -20C: 1.0mm

		observed	
		yes	no
forecast	yes	32	5
	no	18	24

POD	64	
FAR	14	
KSS	47	
CSI	58	
Avg LT (min)		7.3

-10 to -15: 1.0mm; -15 to -20C: 1.25mm

		observed	
		yes	no
forecast	yes	29	4
	no	21	25

POD	58	
FAR	12	
KSS	44	
CSI	54	
Avg LT (min)		7

-10 to -15: 1.25mm; -15 to -20C: 1.0mm

		observed	
		yes	no
forecast	yes	32	5
	no	18	24

POD	64	
FAR	14	
KSS	47	
CSI	58	
Avg LT (min)		7.3

-10 to -15: 1.25mm; -15 to -20C: 1.25mm

		observed	
		yes	no
forecast	yes	28	4
	no	22	25

POD	56	
FAR	13	
KSS	42	
CSI	52	
Avg LT (min)		7

-10 to -15: 1.5mm; -15 to -20C: 1.0mm

		observed	
		yes	no
forecast	yes	32	5
	no	18	24

POD	64	
FAR	14	
CSI	58	
KSS	47	
Avg LT (min)		7.3

-10 to -15: 1.5mm; -15 to -20C: 1.25mm

		observed	
		yes	no
forecast	yes	27	4
	no	23	25

POD	54	
FAR	13	
CSI	50	
KSS	40	
Avg LT (min)		6.9

Appendix

2X2 forecast matrices used in the development of the two-layer LVIL CG forecast algorithm. POD - Probability of Detection, FAR - False Alarm Rate, KSS - Kuipers Skill Score, LT - Leadtime

-10 to -15: 0.1mm; -15 to -20C: 1.5mm

		observed	
		yes	no
forecast	yes	27	4
	no	23	25

POD	54
FAR	13
KSS	40
CSI	50
Avg LT (min)	6.9

-10 to -15: 0.25mm; -15 to -20C: 1.5mm

		observed	
		yes	no
forecast	yes	27	4
	no	23	25

POD	54
FAR	13
KSS	40
CSI	50
Avg LT (min)	6.8

-10 to -15: 0.5mm; -15 to -20C: 1.5mm

		observed	
		yes	no
forecast	yes	26	3
	no	24	26

POD	52
FAR	10
KSS	42
CSI	49
Avg LT (min)	6.7

-10 to -15: 0.75mm; -15 to -20C: 1.5mm

		observed	
		yes	no
forecast	yes	26	3
	no	24	26

POD	52
FAR	10
KSS	42
CSI	49
Avg LT (min)	6.7

-10 to -15: 1.0mm; -15 to -20C: 1.5mm

		observed	
		yes	no
forecast	yes	26	3
	no	24	26

POD	52
FAR	10
KSS	42
CSI	49
Avg LT (min)	6.7

-10 to -15: 1.25mm; -15 to -20C: 1.5mm

		observed	
		yes	no
forecast	yes	25	3
	no	25	26

POD	50
FAR	11
KSS	40
CSI	47
Avg LT (min)	6.7

-10 to -15: 1.5mm; -15 to -20C: 1.5mm

		observed	
		yes	no
forecast	yes	25	3
	no	25	26

POD	50
FAR	11
CSI	47
KSS	40
Avg LT (min)	6.7

REFERENCES

Boyd, B.F., W.P. Roeder, J.B. Lorens, D.S. Hazen and J.W. Weems, 1995: Weather support to pre-launch operations at the Eastern Range and Kennedy Space Center. *6th Conf. on Aviation Wea. Sys.*, Dallas, 15-20 Jan 95, 135-140.

Breed, D.W., and J.E. Dye, 1989: The electrification of New Mexico thunderstorms, Part II, Electric field growth during initial electrification. *J. Geophys. Res.*, 94, 14841-14854.

Buechler, D.E., and S.J. Goodman, 1990: Echo size and asymmetry: Impact on NEXRAD storm identification. *J. Appl. Meteor.*, 29, 962-969.

Crum, T.D., R.L. Alberty, and D.W. Burgess, 1993: Recording, archiving, and using WSR-88D data. *Bull. Amer. Meteor. Soc.*, 44, 9-79.

Doswell, C.A., R. Davies-Jones, and D.L. Keller, 1990: On summary measures of skill in rare event forecasting based on contingency tables. *Wea Forecasting*, 5, 576-585.

Dye, J.E., J.J. Jones, W.P. Winn, T.A. Cerni, B. Gardiner, D. Lamb, R.L. Pittner, J. Hallett, and C.P.R. Saunders, 1986: Early electrification and precipitation development in a small, isolated Montana cumulonimbus. *J. Geophys. Res.*, 91, 1231-1247.

_____, W.P. Winn, J.J. Jones, and D.W. Breed, 1989: The electrification of New Mexico thunderstorms, Part I, Relationship between precipitation and development and the onset of electrification. *J. Geophys. Res.*, 94, 8643-8656.

Federal Meteorological Handbook 11, 1991: Doppler Radar Meteorological Observations Part C. Office of the Federal Coordinator for Meteorological Services and Supporting Research, U.S. Department of Commerce/National Oceanic and Atmospheric Administration, Washington D.C.

Greene, D.R., and R.A. Clark, 1972: Vertically integrated liquid water – A new analysis tool. *Mon. Wea. Rev.*, 100, 548-552.

Gremillion, M.S., 1998: Thunderstorm characteristics of cloud-to-ground lightning at the Kennedy Space Center, Florida: A study of lightning initiation signatures as indicated by doppler radar. *M.S. Thesis*, Florida State University, May 1998, 109 pp.

Hanselman, D., and B. Littlefield, 1996: *Mastering MATLAB 5*. Prentice Hall, 638 pp.

Heckman, S., 1999: An optimal relation of radar reflectivity to lightning rate. *11th Conf. Atmos. Elec.*, Gunterville, AL, 7-11 Jul 99, 719-721.

Hodanish, S., D. Sharp, W. Collins, C. Paxton, and R.E. Orville, 1997: A 10-yr monthly lightning climatology of Florida: 1986-95. *Wea. Forecasting*, 12, 439-448.

Hondl, K.D., and M.D. Eilts, 1994: Doppler radar signatures of developing thunderstorms and their potential to indicate the onset of cloud-to-ground lightning. *Mon. Wea. Rev.*, 122, 1818-1836.

Idone, V., D. Davis, P. Moore, Y. Wang, R. Henderson, M. Ries, and P. Jamason, 1998b: Performance Evaluation of the U.S. National Lightning Detection Network in Eastern New York 1. Detection efficiency.. *J. Geophys. Res.*, 103, 9045-9055

_____, 1998b: Performance Evaluation of the U.S. National Lightning Detection Network in eastern New York 2. Location accuracy. *J. Geophys. Res.*, 103, 9057-9069.

Jameson, A.R., M.J. Murphy, and E.P. Krider, 1996: Multiple-parameter radar observations of isolated Florida thunderstorms during the onset of electrification. *J. Applied Meteor.*, 35, 343-354.

Johnson, J.T., P.L. MacKeen, A. Witt, E.D. Mitchell, G.J. Stumpf, M.D. Eilts, and K.W. Thomas, 1998: The storm cell identification and tracking algorithm. *Wea. Forecasting*, 13, 263-276.

Lopez, R.E., and R.L. Holle, 1987: Study of the interaction between the sea breeze and the synoptic flow using lightning data. *17th Conf. on Hurricanes and Trop. Meteor.*, Miami, 7-10 Apr 87, 82-85.

Marshall, J.S., and W.M. Palmer, 1948: The distribution of raindrops with size. *J. Meteor.*, 5, 165-166.

McKibben, L., 1995: WSR-88D algorithm testing and display system (WATADS) Reference guide. *Systems Management and Radar technology Group*, National Severe Storms Laboratory, 111 pp.

Michimoto, K., 1991: A study of radar echoes and their relation to lightning discharge of thunderclouds in the Hokuriku District, Part I: Observation and analysis of thunderclouds in summer and winter. *J. Meteor. Soc. Japan*, 69, 327-335.

_____, 1993: A study of radar echoes and their relation to lightning discharge of thunderclouds in the Hokuriku District, Part II: Observation and analysis of "single flash" thunderclouds in midwinter. *J. Meteor. Soc. Japan*, 71, 195-204.

Neumann, C.J., 1968: Frequency and duration of thunderstorms at Cape Kennedy, Part 1. ESSA Tech. Memo. WBTM SOS-2, 34 pp. [US Department of Commerce, Springfield, VA].

_____, 1971: The thunderstorm forecasting system at the Kennedy Space Center. *J. Applied Meteor.*, 10, 921-936.

Pinder, C.S, 1998, Internal 45th Weather Squadron Memo, 45th Weather Squadron, 1201 Minuteman St., Patrick AFB, FL, 32925.

Press, W.H., S.A. Teukolsky, W.T. Vetterling, and B.P. Flannery, 1992: *Numerical Recipes in Fortran*. Cambridge University Press, 963 pp.

Rao, P.A., H.E. Fuleberg, and K.K. Droegemeier, 1999: High resolution modeling of the Cape Canaveral land/water circulations and associated features, *Mon. Wea. Rev.*, 127, 1808-1821.

Robinson, M., and M.I. Biggerstaff, 1997: Relationship between reflectivity profiles, cloud-to-ground lightning, and storm system characteristics for convective cells in a coastal zone. *28th Conf. Radar Meteor.*, Austin, 153-154.

Roeder, W.P., 2000, Personal Communication, Discussion of operational needs of KSC as related to CG lightning, 45th Weather Squadron, 1201 Minuteman St., Patrick AFB, FL, 32925.

Roeder, W.P., and D.E. Harms, 2000: Using climatology to improve weather forecasting for America's space program. *12th Conf. on Applied Climo.*, Asheville, NC, 7-11 May 00. 4 pp.

_____, and C.S. Pinder, 1998: Lightning forecasting empirical techniques for central Florida in support of America's space program. *16th Conf. on Wea. Anal. and Forecasting*, Phoenix, 11-16 Jan 98, 475-477.

Schaefer, J.T., 1990: The critical success index as an indicator of warning skill. *Wea. Forecasting*, 5, 570-575.

Unidata Tutorial, 2000: GARP User's Guide. http://www.unidata.ucar.edu/packages/gempak/examples/

Wilks, D.S., 1995: *Statistical Methods in the Atmospheric Sciences*. Academic Press, 467 pp.

Ziegler, C.L., P.S. Ray, and D.R, MacGorman, 1986: Relations of kimematics, microphysics, and electrification in an isolated mountain thunderstorm, *J. Atmos. Sci.*, 43, 2098-2114.

Zipser, E.J., and K. Lutz, 1994: The vertical profile of radar reflectivity of convective cells: A strong indicator of storm intensity and lightning probability? *Mon. Wea. Rev.*, 122, 1751-1759.